CrossMark

Simplified analysis of a generalized bias test for fabrics with two families of inextensible fibres

M. Cuomo⬤, F. dell'Isola⬤ and L. Greco

Abstract. Two tests for woven fabrics with orthogonal fibres are examined using simplified kinematic assumptions. The aim is to analyse how different constitutive assumptions may affect the response of the specimen. The fibres are considered inextensible, and the kinematics of 2D continua with inextensible chords due to Rivlin is adopted. In addition to two forms of strain energy depending on the shear deformation, also two forms of energy depending on the gradient of shear are examined. It is shown that this energy can account for the bending of the fibres. In addition to the standard bias extension test, a modified test has been examined, in which the head of the specimen is rotated rather than translated. In this case more bending occurs, so that the results of the simulation carried out with the different energy models adopted differ more that what has been found for the BE test.

Mathematics Subject Classification. 74A30 (Nonsimple materials) · 74K15 (Membrane) · 74E30 (Composite and mixture properties).

Keywords. Generalized continua · Second gradient elasticity · Woven composites · Normalization method · Bias test.

1. Introduction and background

In the past decades there has been an impressive progress in the development of new materials for mechanical related applications. The design and the modeling of new materials has become one of the leading challenges for the research in engineering, together with the need of improving existing structural analysis methods in order to take advantage of all the innovations introduced. Fibre composite materials have traditionally introduced strong innovation in the manufacturing industries, ranging from transportation to construction industries. Long fibre composites are constituted by unidirectional fibres, and their major effect is to improve the mechanical properties of the material in that direction, causing significant anisotropy. New generations of composites have been developed, that can offer advantages over the unidirectional fibre-reinforced mats commonly used. Woven and non-woven fabrics are now extensively used in several applications, either as reinforcement or as structural material per se (see, e.g. [1–3]). On the other hand, this type of 'material' is present in nature also in some biological tissues [4–7]. Woven fabrics guarantee dimensional stability, balanced properties in the reinforcement plane, high impact resistance, good drapability, and suitability for manufacturing of doubly curved components.

Woven fabrics are produced by mechanically bonding together two or more fibre bundles (also known as yarns) in a specific architecture. The fabric's integrity is maintained by the mechanical interlocking of the fibres. According to the type of weave, 2D or 3D fabric can be obtained.

Usually high-performance materials are used for the fibres (e.g. carbon, glass, and high polymers), so that woven fabrics can be considered almost inextensible in the warp and weft directions and mainly deform for shear presenting a strong geometric hardening. More complex is the behaviour of three-dimensional woven fabrics, for which the deformation in the transverse direction depends not only on the geometry of the fabric, but also on friction and interlocking among them. Friction and slippage of fibres is also a major issue in plane fabrics, when the deformation becomes large. In this context, some significant studies are dealt with in [8,9].

The characterization of the mechanical response of woven composites and its modeling is one of the most challenging and debated issues in material engineering. The problem is very complex since it involves many non standard tasks, primarily due to the fact that the material we are dealing with is not a simple material in the sense that its micromechanics strongly influences the observable behaviour, and cannot be disregarded in the simulations. Some relevant aspects related to parameter identification of similar complex materials are analysed in [10,11]. Besides, other significant issues as contact–impact problems or damage evolution and identification are studied in [12–16].

Tests for evaluating the stiffness of fabrics are suggested by many standards, like ASTM D 3518 and D4255, EN ISO 13934-1. Since shearing is the most important deformation mode of plane woven fabrics test have been specifically developed for characterizing their shear response. Three methods are most commonly used for determining the fabric shear properties, each one of them having benefits and drawbacks, the direct shear (one rail or two rails set-ups are employed) (DS), the picture frame test (PF), and the uniaxial bias extension test (BE) [17–20]. In all these methods, the phenomena of shear locking and specimen buckling (wrinkling) may occur, so that particular care has to be taken in interpreting the results (see, e.g. [21–29] for some analytic and numerical tools which are useful to address this issue). Also biaxial extension tests are performed on woven composites, in which case locking does not occur. In the DS test in order to avoid wrinkling some amount of tension has to be applied. A nearly homogeneous shear state is reached in the PF test but it is extremely sensitive to specimen misalignment issues [30,31]. By contrast, the BE test is relatively insensitive to specimen misalignment, but a non-homogenous deformation state is produced in the sample, making more difficult to interpret the results. In addition, at high shear strains, a critical shear angle is reached when the threads in the central part of the specimen are so closely packed that any increase in tension causes lateral compression and consequently wrinkling. At higher extension, the shear deformation locks, and sliding of the threads is observed [32]. However, the BE test, being very simple to perform, since it does not require any special fitting and can be performed on any standard extension testing apparatus, is probably the most used test.

The bias extension test is an extensional test on a strip of the woven fabric constituted by two families of fibres oriented at 45° with respect to the axis of the specimen, clamped at the ends (see Fig. 1). The load elongation curve is recorded, and in order to obtain information on the shear stiffness, or on the shear stress exerted in the specimen, it is necessary to treat the data obtained from the testing apparatus. Normalization methods have been proposed for interpreting the data from the test, based on simplifying assumptions related to the kinematic response and to the material behaviour.

Theories have been proposed to normalize the data for rate-independent fabrics and also for viscous fabrics [17,33–38]. Starting from a simplified kinematics, the shear strain in the sample is related to the
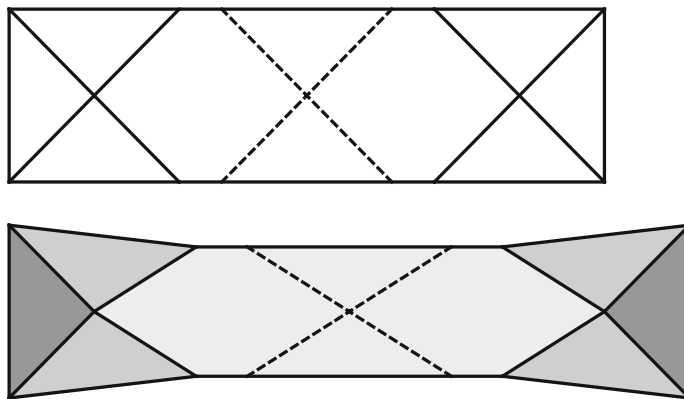

Fig. 1. Initial configuration of the sample (*top*) and its current configuration (*bottom*) in a BE test

external extension, then equating the external power to the internal one a relation between the shear stress and strain is obtained. In addition to the kinematic assumption, extra hypotheses are introduced on the internal power in order to get the desired result. Most but not all the normalization theories proposed ignore the effects of shear tension coupling (that is, the fact that the shear stiffness of biaxial woven fabrics appears to increase with increasing tensile stress along the fibre directions probably due to friction) [38–42].

A numerical simulation of the test is a critical task in order to develop a realistic mechanical model of the composite material, able to be employed in the analysis of more complex geometries. The hypotheses introduced in the normalization procedures do not appear to be realistic enough, so that the results obtained on the basis of these methods are little more then conventional. A numerical analysis of the extension bias test was discussed in [43,44]. A 2D continuum was employed to which homogenized material properties were attributed, that accounted for the presence of two families of strictly inextensible fibres. In literature there are many examples of homogenization procedures which have the purpose of obtaining a bulk macro model starting from a proper kinematical description at micro-scale (see, e.g. [45–53]). The results of Pipkin and Rivlin concerning the deformation of nets with inextensible chords were used in order to derive the kinematics of the model [54–56]. It was found that first gradient deformation model produce sharp discontinuities in the fibre rotations, that are not observed in the experiments. Therefore it was suggested, in accordance with what proposed by [57–63] to employ higher-order deformation models (see, e.g. [64–66]), able to simulate the bending energy stored in the fibres at the mesolevel. Several energy models were analysed, with the intent of matching the experimental observations. In the same spirit, it is possible to exploit the micro-polar surface theory; indeed, higher-order deformation models with proper assumption [67] can be interpreted in the framework of micro-structured or micro-polar materials (see, e.g. for further details [68–74]). As a note, we remark that to perform numeric simulations involving higher gradient models, *ad hoc* tools are to be employed because standard C^0 FEM are not optimized for this purpose (see, e.g. [75–79]).

It was found, however, that qualitatively the response of the specimen to the extension was similar for all the energy models employed, so that in a real experiment it would be difficult to differentiate among them, and primarily to assess the relative relevance of the second-order bending energy in the deformation process.

The bias extension test, indeed, allows to simulate one mode of deformation only, for a very particular geometry. The consideration of geometrical settings with different boundary conditions can be useful to discriminate among the possible constitutive models applicable to the material. Aim of this work is to analyse the simulations of a generalized bias test. In it the geometry of the sample is the same as for the standard test, but a boundary displacement different than a simple extension is applied. Specifically, a rotation of the free end of the specimen around one of the corners will be examined (see Fig. 15). As it will be shown, and as will be discussed in a forthcoming paper [44] the response of the specimen may present phenomena that are not present in the standard bias test, as the complete closure of the angle formed between the two families of fibres in a limited zone of the specimen, that may give rise to instabilities. The numerical analysis and the predictions obtained with the simulations yield therefore valuable information for interpreting the experimental results, and for indicating the critical geometrical quantities that need to be measured during the test. In the paper it will be performed a geometrically simplified analysis of both the standard BE test and the newly proposed test, including on the analysis the effect of the second gradient energy.

First the assumptions employed for the model will be presented and briefly discussed. Them the standard BE test will be examined, in order to extend the normalization procedures proposed in the literature for including the effect of second gradient deformation. The analysis of the new test will follow a similar reasoning, for the tests examined will be presented the predictions obtained using some simple strain energy models, on the assumption that no damage occurs.

2. Assumptions of the model

We consider a plane balanced composite constituted by two orthogonal families of woven fibres. We introduce the following assumptions regarding the material model:

H1 An average equivalent thickness is considered for the composite, that we assume to be constant throughout, so that the material can be treated as an equivalent 2D continuum.

H2 The fibres are inextensible.

Introducing a local reference frame attached to the fibre directions, and denoting by $\mathbf{P} = \{\xi^1, \xi^2\}$ the coordinates of a point of the specimen in this frame (see Fig. 2), its basis vectors are

$$\mathbf{D}_1 := \frac{\mathrm{d}\mathbf{P}}{\mathrm{d}\xi^1}, \quad \mathbf{D}_2 := \frac{\mathrm{d}\mathbf{P}}{\mathrm{d}\xi^2} \tag{1}$$

From the inextensibility assumption it follows that these directors can undergo only a rigid rotation upon deformation of the continuum. Denoting by $\mathbf{d}_1, \mathbf{d}_2$ the deformed directors it follows that:

$$\mathbf{d}_1(\xi^1) := \mathbf{R}_1\left(\vartheta_1\left(\xi^1\right)\right)\mathbf{D}_1 = \cos\left(\vartheta_1\left(\xi^1\right)\right)\mathbf{D}_1 + \sin\left(\vartheta_1\left(\xi^1\right)\right)\mathbf{D}_2,$$
$$\mathbf{d}_2\left(\xi^2\right) := \mathbf{R}_2\left(\vartheta_2\left(\xi^2\right)\right)\mathbf{D}_2 = \sin\left(\vartheta_2\left(\xi^2\right)\right)\mathbf{D}_1 + \cos\left(\vartheta_2\left(\xi^2\right)\right)\mathbf{D}_2. \tag{2}$$

where $\mathbf{R}_1$ and $\mathbf{R}_2$ are in plane unit rotation operators, depending on the rotation angles ϑ_1, ϑ_2. It was proved by Rivlin [56] that in the present hypotheses the two rotation angles depend only on the respective parametric abscissa, as highlighted in Eq. (2). The constrained gradient deformation tensor becomes

$$\mathbf{F}_R := \left(\mathbf{R}_1\left(\vartheta\left(\xi^1\right)\right)\mathbf{D}_1\right)\otimes\mathbf{D}^1 + \left(\mathbf{R}_2\left(\vartheta\left(\xi^2\right)\right)\mathbf{D}_2\right)\otimes\mathbf{D}^2, \tag{3}$$
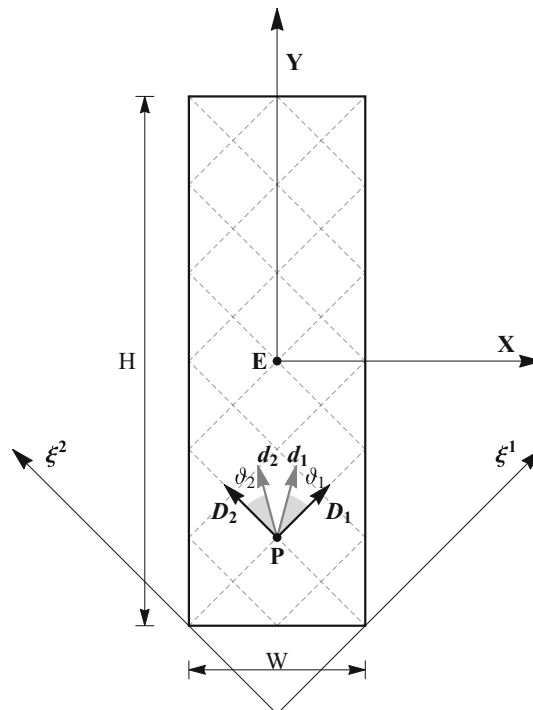

Fig. 2. Initial configuration B_0 and its inextensible director

We have therefore $\mathbf{d}_i \cdot \mathbf{d}_i = 1$, $i = 1, 2$, and we define

$$\gamma = \mathbf{d}_1 \cdot \mathbf{d}_2 = \sin(\vartheta_1 + \vartheta_2). \tag{4}$$

The Cauchy strain tensor is than

$$\mathbf{C} := \mathbf{D}_1 \otimes \mathbf{D}_1 + \gamma \mathbf{D}_1 \otimes \mathbf{D}_2 + \gamma \mathbf{D}_2 \otimes \mathbf{D}_1 + \mathbf{D}_2 \otimes \mathbf{D}_2, \tag{5}$$

while the Green strain tensor is given by

$$\mathbf{E} := \frac{\gamma}{2}(\mathbf{D}_1 \otimes \mathbf{D}_2 + \mathbf{D}_2 \otimes \mathbf{D}_1). \tag{6}$$

Next assumptions regard the material constitutive behaviour.

H3 It is assumed that the material deforms elastically, that is, no damage or any other kind of dissipation mechanism is considered. Therefore there exists an internal energy given by the elastic strain potential. This assumption could be relaxed in the case that only monotonic load histories are considered, like is the case in the present work. However, for the sake of simplicity, we keep the assumption in the present form.

H4 According to the discussion of Sect. 1, the strain energy is assumed as the sum of two independent contributions, the first that depends on Green's strain tensor (first gradient energy), the second that depends on the gradient of the strain (second gradient energy):

$$\mathfrak{F} := \alpha_1 \int_B g_1(\mathbf{E}) \, \mathrm{d}B + \alpha_2 \int_B g_2(\nabla \mathbf{E}) \, \mathrm{d}B \tag{7}$$

where α_1 and α_2 are constitutive weight parameters.

In the case of in plane deformation, the only non-vanishing invariant of Green's tensor is the second invariant $I_2 := \frac{\gamma^2}{2}$, so that any isotropic first gradient energy functional must be a function of γ^2. Since the basis vector are constant, the only non-vanishing terms of the gradient of the strain tensor $\nabla \mathbf{E}$ are

$$(\nabla \mathbf{E})_{121} = (\nabla \mathbf{E})_{211} = \frac{\cos(\vartheta_1 + \vartheta_2)}{2} \frac{\mathrm{d}\vartheta_1}{\mathrm{d}\xi^1},$$
$$(\nabla \mathbf{E})_{122} = (\nabla \mathbf{E})_{212} = \frac{\cos(\vartheta_1 + \vartheta_2)}{2} \frac{\mathrm{d}\vartheta_2}{\mathrm{d}\xi^2} \tag{8}$$

The second gradient energy term is assumed to be a function of the norm of the strain gradient, so that we have:

$$\mathfrak{F} = \alpha_1 \int_B g_1(\gamma^2) \, \mathrm{d}B + \alpha_2 \int_B g_2(\|\nabla \mathbf{E}\|) \, \mathrm{d}B$$
$$\|\nabla \mathbf{E}\| = \cos^2(\vartheta_1 + \vartheta_2) \left[\left(\frac{\mathrm{d}\vartheta_1}{\mathrm{d}\xi^1}\right)^2 + \left(\frac{\mathrm{d}\vartheta_2}{\mathrm{d}\xi^2}\right)^2 \right] \tag{9}$$

2.1. Energy models

In the following developments, in order to test the influence of different constitutive models on the overall response of the specimen to the imposed displacement, some energy models will be used, selected in such a way as to be representative of the deformation phenomena occurring in the material.

Two forms are considered for the first gradient strain energy. In the first case, the strain energy g_1 is taken quadratic in γ, i.e. $g_{1,1} = \frac{1}{2}k\gamma^2$; this corresponds to an hyperelastic continuum. In the second one, the strain energy is directly related to the square of the relative rotation of the fibres, $g_{1,2} = \frac{1}{2}k\left(\frac{\pi}{2} - \cos^{-1}\gamma\right)^2 = \frac{1}{2}k(\vartheta_1 + \vartheta_2)^2$. The latter mechanism can be related to the friction existing between the fibres in the contact point. Due to the initial curvature of the fibres, an increment in the
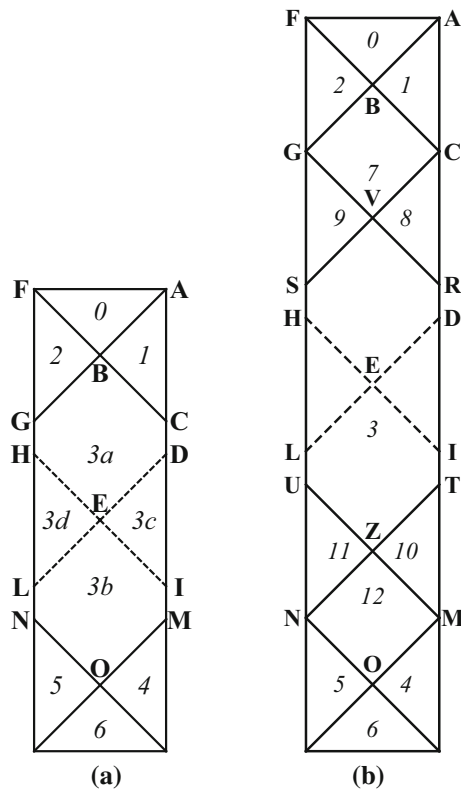
FIG. 3. Bias Extension test. Geometry of the specimen. In *italics* are indicated the numbers of the regions of homogeneous deformation. **a** Geometry of the specimen for the Bias Extension test. $H/W < 4$. **b** Geometry of the specimen for the Bias Extension test. $4 < H/W < 6$

tensile stress of the fibres results into an increase in the contact force between the fibres, hence to an increase of the friction resistance to relative rotation. Experimentally it appears that this effect results in a nonlinear dependency of the shear force on the tensile stress of the fibres, but, due to the lack of specific information, this effect is here disregarded.

Also for the second gradient strain energy, two models are considered. In the first case, the strain energy $g_{2,1}$ is taken directly proportional to the square of the norm of the gradient of the strain tensor, Eq. (8). In the second case, $g_{2,2}$ is taken proportional to the square of the gradient of the rotations of the fibres, that is, in the expressions (8) of the strain gradient it is assumed $\cos(\vartheta_1 + \vartheta_2) = 1$.

2.2. Geometry of the specimen and simplified kinematics

In the paper, we consider a standard specimen employed in the BE tests, that is, a strip of composite with the fibres at 45° from the specimen axis. The ratio between the length and the width of the specimen (the slenderness ratio) is denoted by $\lambda = H/W$ (see Fig. 2). The lower end of the specimen is fixed, while the upper end is subjected to rigid translations (case 1) or to a rigid rotation around the corner (case 2).

The origin of the reference frame x, y is set in the centre of the specimen, with the y axis aligned along the specimen axis.

In order to obtain, for the cases considered in next sections, a close form solution for the deformation field, an additional hypothesis is introduced, whose validity is by far more approximated than the kinematic assumption of inextensible fibres. The geometric assumption is that the fibres remain straight,

except along lines where concentrated kinks may occur. This assumption is commonly employed in the discussion of experimental results [17,35,42].

As a consequence, the specimen gets subdivided in discrete regions of constant shear deformation, shown in Fig. 3 for the cases $H/W < 4$ and $4 < H/W < 6$. Note that in regions 0 and 6 the shear is zero (since they are triangles whose sides do not elongate), that is those regions can only undergo a rigid motion.

3. The standard Bias Extension test

The free end of the sample is subjected to a translation v along the y-axis. the deformation of the sample depends on the slenderness ratio H/W, which determines the number of internal regions in which the shear is homogeneous, as shown in Fig. 4. For $2 \leq H/W < 4$ only one region of homogeneous shear can exist in the interior of the specimen (region 3), so that in this case, due to symmetry considerations, the deformed configuration of the specimen is uniquely determined by geometric conditions, as illustrated in Fig. 4a. For $4 \leq H/W < 6$ at the interior of the specimen there exist three regions with different constant deformation (regions 3,7,12), plus the transition zones, Fig. 4b, so that the deformation is not uniquely determined by geometric considerations and it has to be determined through a mechanical analysis. For greater slenderness ratios more regions of homogeneous deformation occur. We shall examine separately
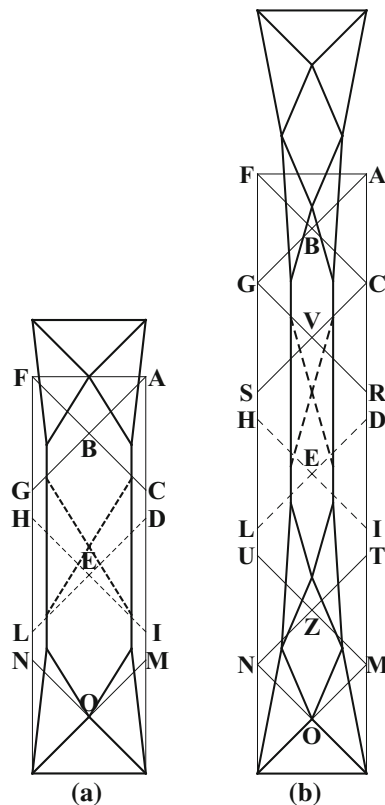

FIG. 4. Bias Extension test. Simplified kinematics. **a** Schematic deformation. $H/W < 4$. **b** Schematic deformation. $4 < H/W < 6$

TABLE 1. *Shear deformation for the Bias Extension test.* $H/W < 4$

Region	γ	Series expansion	$\theta_1 + \theta_2$
3	$\frac{d(d+2H-2W)}{(H-W)^2}$	$\frac{2d}{H-W} + \frac{d^2}{(H-W)^2}$	$\frac{\pi}{2} - \arccos(2\gamma_3)$
1	$\frac{d+H-W-\sqrt{(H-W)^2-2d(H-W)-d^2}}{2(H-W)}$	$\frac{d}{H-W} + \frac{d^2}{(H-W)^2} + \frac{d^3}{2(H-W)^3}$	$\frac{\pi}{2} - \arccos(2\gamma_1)$

the cases of $2 \le H/W < 4$ and $4 \le H/W < 6$ in order to highlight the influence of the slenderness of the specimen on the results of the test.

3.1. Case $2 \le H/W < 4$

First we analyse the case $2 \le H/W < 4$. As shown in Fig. 4a, the centre point E undergoes a displacement of $v/2$ along the y-axis, and the shear deformation in the specimen is constant in the central area (region 3), while in the triangular regions 1,2,4,5 the relative rotations between the two families of fibres is half than in the central area. The rotation angle of the fibres in the central area can easily be obtained by the condition that the projections on the specimen axis of the fibre segments BC, OM, ED, EI, and of the parts of the fibres contained between points C, D and I, M be equal to the distance between points O and B in the deformed configuration, i.e.

$$2\|BC\|\cos\theta + 2\frac{H-2W}{\sqrt{2}}\cos\theta = H - W + v$$

$$\cos\theta = \frac{v+H-W}{\sqrt{2}(H-W)} = \frac{v}{\sqrt{2}W(\lambda-1)} + \frac{1}{\sqrt{2}} \tag{10}$$

so that

$$\gamma = \cos\left[2\cos^{-1}\left(\frac{v}{\sqrt{2}W(\lambda-1)} + \frac{1}{\sqrt{2}}\right)\right] \tag{11}$$

This formula is often used in the interpretation of the experimental results. The shear deformations $C_{12} = \mathbf{d}_1 \cdot \mathbf{d}_2$ in the two regions of homogeneous strain 1 and 3 are reported in Table 1, together with their power expansion up to the order 3, showing that $\gamma_1 = \gamma_3/2$ up to the second order. A limit locking displacement is attained in this case, when the fibres in the central region get aligned, that is when $\gamma_3 = 1$, given by

$$v_{lim} = \left(\sqrt{2} - 1\right)(H - W). \tag{12}$$

Denoting by F the reaction force at the clamped end of the specimen and equating the external power to the internal power, the following expression is obtained:

$$F\dot{v} = T(\gamma_3)\dot{\gamma}_3 + T(\gamma_1)\dot{\gamma}_1$$

$$F\dot{v} = \left(T(\gamma_3)2\frac{d+H-W}{(H-W)^2} + T(\gamma_1)\frac{d+H-W+\sqrt{(H-W)^2-2d(H-W)-d^2}}{2(H-W)\sqrt{(H-W)^2-2d(H-W)-d^2}}\right)\dot{v} \tag{13}$$

where T is the shear force per unit length (that is, integrated over the thickness) in the sheet. From expression (13) the relationship between the shear force and the shear strain can be estimated. Expression (13) is not the same usually reported in experimental works (see, e.g. [17]) since the full nonlinear expression has been used in this case. Notice that the shear force $\mathbf{T}$ as obtained is a component of the the second Piola–Kirchhoff stress tensor. Analogous expressions can be obtained using other stress measures.

The use of formula (13) is limited to the hypotheses under which it has been obtained, that is, homogeneous deformations within the specimen regions, straight and inextensible fibres, absence of instability or damage. These conditions of course are not met in actual experiments, so that only rough estimates
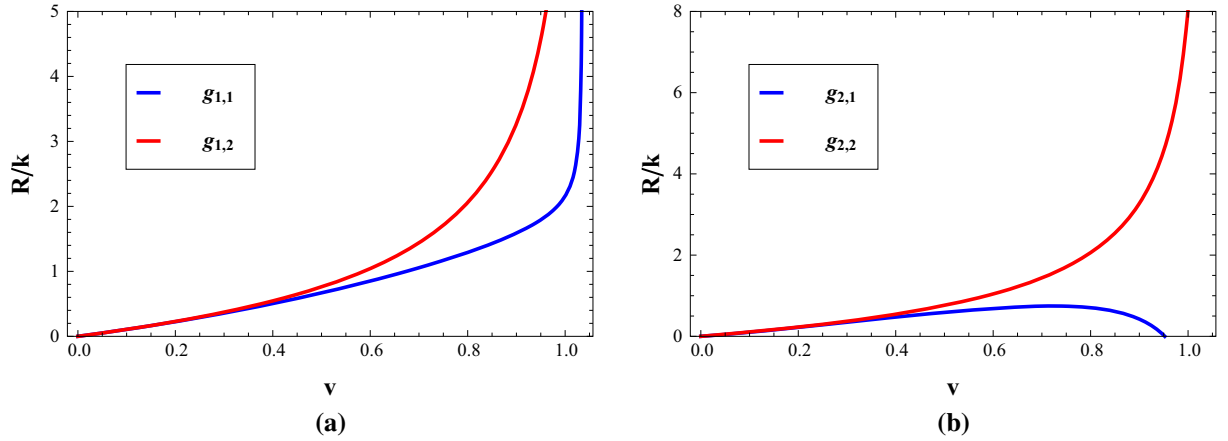
FIG. 5. Bias Extension test. Simulations of the test with first (**a**) and second (**b**) gradient strain energy. **a** Force versus displacement for the extension bias test. $H/W < 4$. First gradient energy. **b** Force versus displacement for the extension bias test. $H/W < 4$. Second gradient energy

can be obtained. We want now to investigate what is the influence of different constitutive models on the load displacement curve obtained within the current hypotheses, in order to evaluate up to what extent valuable information can be obtained from the approximated model. The forms of energy introduced in Sect. 2 are used. The first gradient energy is simply obtained integrating the elastic potential over the volume, and, since the shear strain is constant in each region of the sample, the internal energy is given by:

$$E_{d1} = \int_V \mathfrak{F}_1 dV = \sum_{i=1}^{6} A_i t_i g_1(\gamma_i) = 4A_T\, t\, g_1(\gamma_1) + A_B\, t\, g_1(\gamma_3) \tag{14}$$

having indicated with t the thickness of the sample, assumed constant, with $A_T = W^2/4$ the area of a triangular region, and with A_B the area of the central region of the sample.

For a given end displacement the deformation field minimizes the potential energy

$$\min_{\theta_1, \theta_2} \left(E_d\left(\gamma\left(\theta_1, \theta_2\right)\right) - F\left(u_y^L\left(\theta_1, \theta_2\right) - v\right)\right) \tag{15}$$

where in the last term the Lagrange multiplier F for the constrained end displacement u_y^L is the reaction force exerted on the specimen. The end displacement u_y^L is given by an integral expression, reported in [44]. Evaluating the derivative of the deformation energy with respect to the imposed displacement v we find:

$$\frac{\partial E_d}{\partial v} = \frac{\partial E_d}{\partial \theta_i}\frac{\partial \theta_i}{\partial v} = F\frac{\partial u_y^L(\theta_i)}{\partial \theta_i}\frac{\partial \theta_i}{\partial v} \tag{16}$$

But, since by the implicit function theorem applied at the constraint $u_y^L(\theta) - v = 0$, we get $\frac{\partial \theta_i}{\partial v} = \left(\frac{\partial u_y^L}{\partial \theta_i}\right)^{-1}$, it follows

$$F = \frac{\partial E_d}{\partial v} \tag{17}$$

that is the statement of Castigliano's theorem. Notice that expression (17) is valid whatever be the form of the strain energy, therefore it holds also in the case a second gradient energy is used.
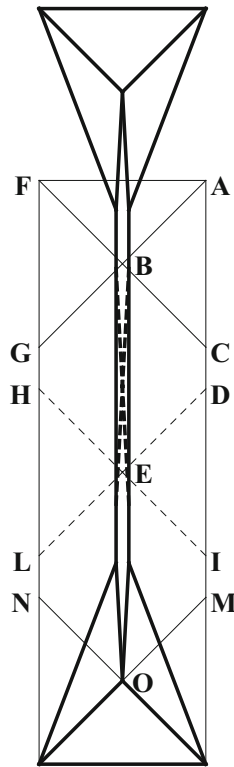
FIG. 6. BE test. Deformation of the sample. $H/W < 4$

In Fig. 5a the load displacement curve is plotted for the two first gradient energy forms considered in Sect. 2.1, $g_{1,1}, g_{1,2}$, normalized with respect to the slope at the origin (that is, the initial slope in both cases is set equal to 1).

The energy $g_{1,1}$, quadratic in the shear strain, presents a smaller initial stiffness with respect to the other case, but in both cases the reaction diverges when the locking displacement is approached. Qualitatively there is little difference between the two cases, that in an experiment could hardly be appreciated.

The deformation of the specimen close to the limit displacement is represented in Fig. 6. It can be appreciated how the central zone of the specimen becomes very narrow, with the fibres aligned, close to what is observed in the experimental results.

In [44] a detailed numerical analysis of the Bias Test was carried out, from which resulted that the shear strain is not constant in the central region of the specimen, contrarily to what have been assumed in the present analysis. In Fig. 7 is presented the relative rotations of the fibres in two points of region 3, i.e. at the centre of the specimen (point E) and at point O as obtained from the numerical analysis (that are not equal), compared with the prediction of the simplified model here presented. Two cases are reported for the numerical results, one for which the strain energy potentials depends on the relative rotation of the fibres and the other for which the strain energy potential depends on the shear γ. The numerical results show little difference from the idealized model, as it is also found in experimental results.

Experimental results on woven fabrics subjected to the BE test show that sharp kinks such as those present in the deformation of Fig. 6 are not observed in the experiments [35], since the fibres bear some flexural rigidity that prevents their curvature to become infinitely large. In [44], it has been proposed to
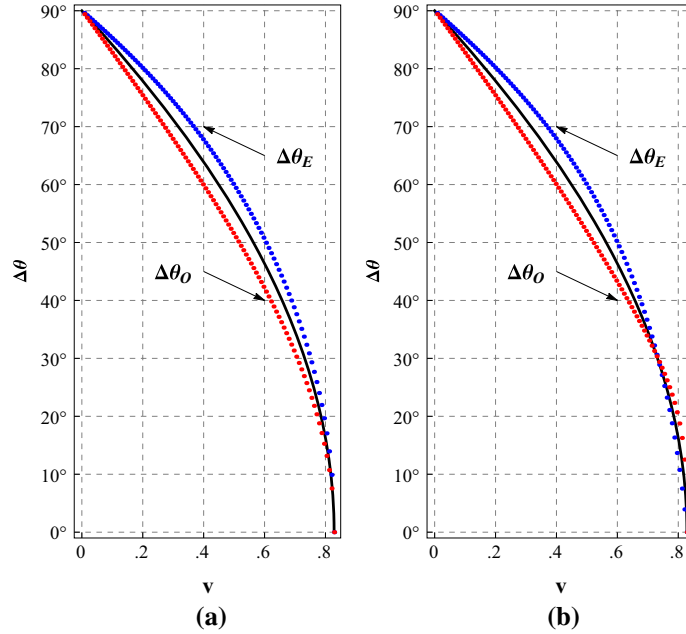
FIG. 7. Bias Extension test H/W=3: comparisons of the theoretical angle incremental evolution with the numerical formulation in [44]. **a** Comparison with the first gradient quadratic energy model. **b** Comparison with the first gradient shear energy model

account for this effect introducing an additional term in the strain energy depending on the gradient of the shear, that, as indicated in Eq. (8), is proportional to the bending curvatures of the two families of fibres. In the limit the bending deformation may be the dominant deformation mode, corresponding to a model of fibres free to rotate but not to bend. In the simplified model presented, in which the shear is piecewise constant, the gradient of the shear may be accounted for considering the relative rotation of the fibres along the edges of the regions of uniform shear, where indeed the experimental results show that the bending of the fibres is more severe. The internal energy then becomes

$$E_{d2} = \sum_{j=1}^{nl} L_j t_j g_2 \left(\Delta \gamma_j \right) = 4\sqrt{2} W t g_2 \left(\gamma_1 - \gamma_3 \right) \tag{18}$$

The contribution to the second gradient energy arise along lines ABG and IOQ, where the rotation θ_1 experiences a jump, and along lines FBC and NOP, where the rotation θ_2 is discontinuous.

The load displacement curves obtained solving problem (15) with the strain energy (18) are plotted in Fig. 5b. Also in this case the results are normalized with respect to the initial slope. While the results obtained with the energy $g_{2,2}$ are similar to those obtained considering first gradient deformation only, the load displacement curve obtained for the energy $g_{2,1}$ presents a limit point, and then an unstable branch, due to the fact that, as noted previously, when the fibres tend to align the gradient of the shear strain vanishes, and the strain energy reaches a maximum for a value of the imposed displacement $\frac{1}{2} \left(\sqrt{3} - 1 \right) (H - W)$, close to the locking limit (see Fig. 8). The reduction in the stiffness of the specimen can account for to the onset of instability in the sample that results into wrinkling. If this hypothesis is correct, the source of instability is a phenomenon related to the second gradient deformation.

The results obtained with all the energy models analysed are summarized in Fig. 9a. Apart from the unstable curve obtained with the energy $g_{2,1}$, no sharp difference exists between the other results, rather the load vs. displacement curve obtained with the first and second gradient strain energies quadratic in
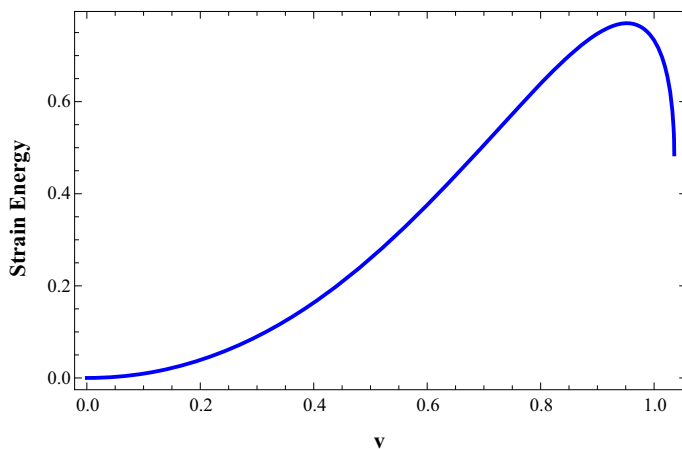
FIG. 8. BE test. Strain energy for the strain gradient model $g_{2,1}$ as function of the imposed displacement. $H/W < 4$
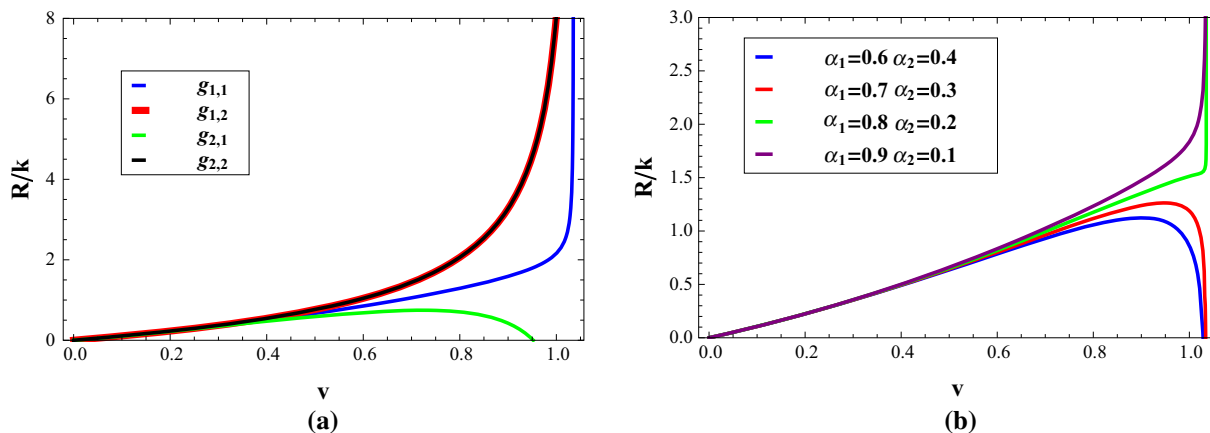

(a) **(b)**

FIG. 9. Bias Extension test. Load versus displacement. **a** Force versus displacement for the Bias Extension test. $H/W < 4$. First and second gradient energy models. **b** Force versus displacement for the Bias Extension test. Strain energy $\alpha_1 g_{1,1} + \alpha_2 g_{2,1}$. $H/W < 4$

the relative rotations perfectly coincide. This is a consequence of the Rivlin kinematics of the inextensible network, for which case the rotation of the i-th fibre depends only on the coordinate ξ^1. Figure 9b shows how the first and second gradient shear energy can combine in order to model a more or less severe transition of the load-displacement curve from the unstable to the stable behaviour close to the locking point.

3.2. Case $4 \leq H/W < 6$

The schematic deformation of the sample is depicted in Fig. 4b. In this case the shear takes different values in region 3 and in regions 7 and 12. Other regions of homogeneous shear are the triangular areas 1, 2, 4, 5 and 8, 9, 10, 11. Hence the deformation of the specimen is not determined by geometric considerations
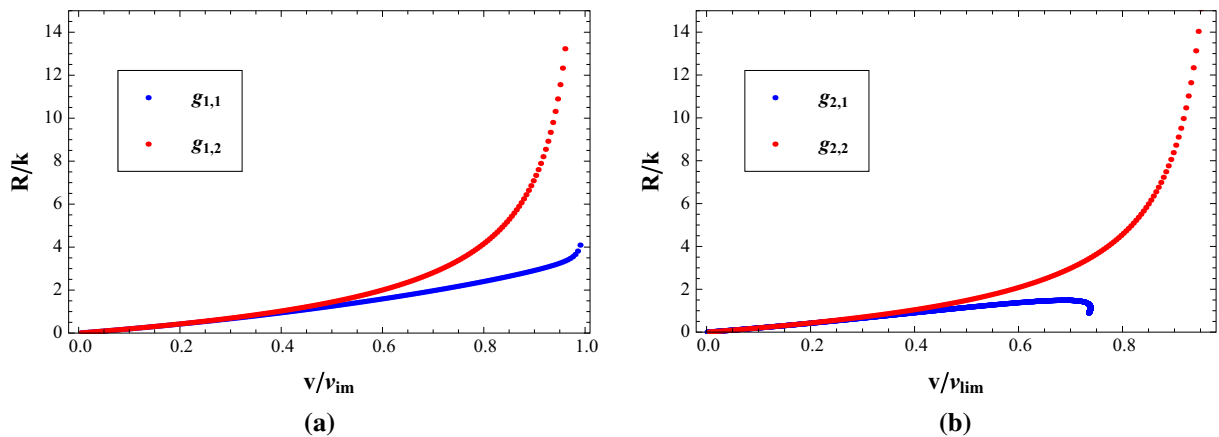
FIG. 10. Bias Extension test. $H/W > 4$. Simulations of the test with first (**a**) and second (**b**) gradient strain energy. **a** Force versus displacement for the extension bias test. $H/W > 4$. First gradient energy. **b** Force versus displacement for the extension Bias Test. $H/W > 4$. Second gradient energy

only, since the coordinates of points V, Z are unknown, and have to be found solving the minimization problem (15).

The results of the calculations are presented in Fig. 10a, b for the first and second gradient energy models respectively after normalization with respect to the initial slope. The load displacement curves are analogous to those obtained for to the previous case of the less slender sample. The limit displacement corresponding to the locking condition is the same as in the previous case $((\sqrt{2} - 1)(H - W))$. The results for the first and second gradient energies quadratic in the rotations (models $g_{1,2}$ and $g_{2,2}$) also in this case are almost coincident—the small difference is due to the non homogeneity if the shear throughout the specimen. All the curves appear similar except for the second gradient energy model depending on the shear strain, that present an unstable behaviour, Fig. 11a. An enlargement of the load-displacement curve for the latter case is shown in Fig. 11b, from which it can be seen that for the slender specimen snap-back occurs. The behavior in the case the second gradient energy dominates, is the more unstable the more slender is the sample, giving rise to a sort of size effect.

In order to verify whether the calculated deformation deviates from uniformity along the specimen, we plot the calculated values of the relative rotations $\theta_1 + \theta_2$ in regions 3, 7. Recall that on the case of the specimen with $H/W < 4$ these two shears were equal. In all graphs is plotted half of the angle formed between the fibres, that goes from 45° to 0°. The results obtained with the first gradient energy models are plotted in Fig. 12. For both first gradient models the relative rotation of the fibres is almost uniform throughout the specimen, as occurs in the case $H/W < 4$, and some difference, leading to a neck in the central area, occurs only for displacements close to the limit one. Comparing these plots to those reported in Fig. 7, it can be observed that the deviation from uniformity of the rotation angles obtained numerically follows the same trend as the one found with the idealized kinematics. In the case of the second gradient energy models, however, the relative rotation of the fibres is not uniform, as represented in Fig. 13, and the difference is particularly relevant when instability arises (Fig. 13a). Figure 14 reports the deformed shapes of the specimen for a displacement close to the limit one obtained using the modelks $g_{1,2}, g_{2,2}$. It can be seen that for the first gradient model the deformation is almost uniform in the central zone, while for the second gradient model a neck appears in the central zone with a smooth variation of the shear angles along the specimen. This difference in the deformation could be useful in the interpretation of the experimental results.
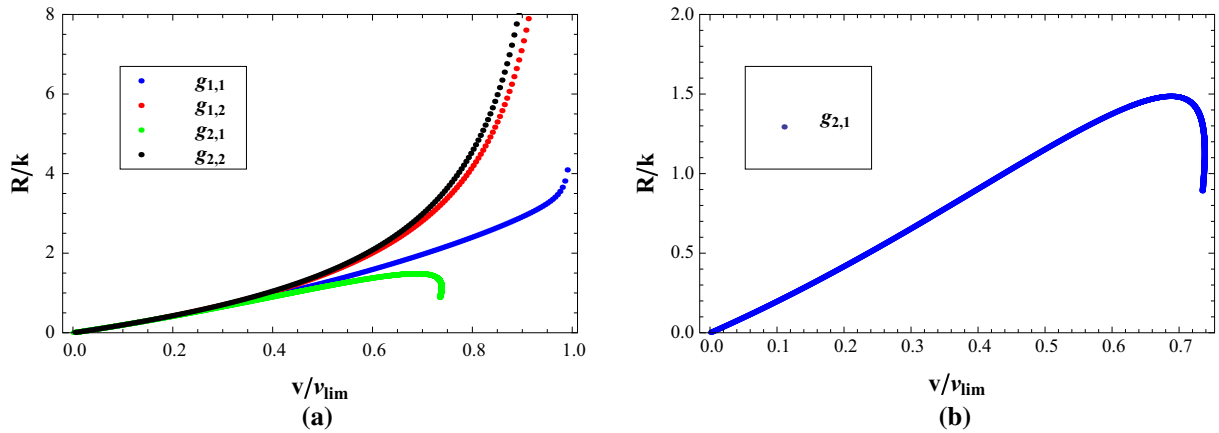
FIG. 11. Bias Extension test. Load versus displacement. Summary of the results. **a** Force versus displacement for the Bias Extension test. $H/W > 4$. First and second gradient energy models. **b** Force versus displacement for the Bias Extension Test. Strain energy $g_{2,1}$. $H/W > 4$
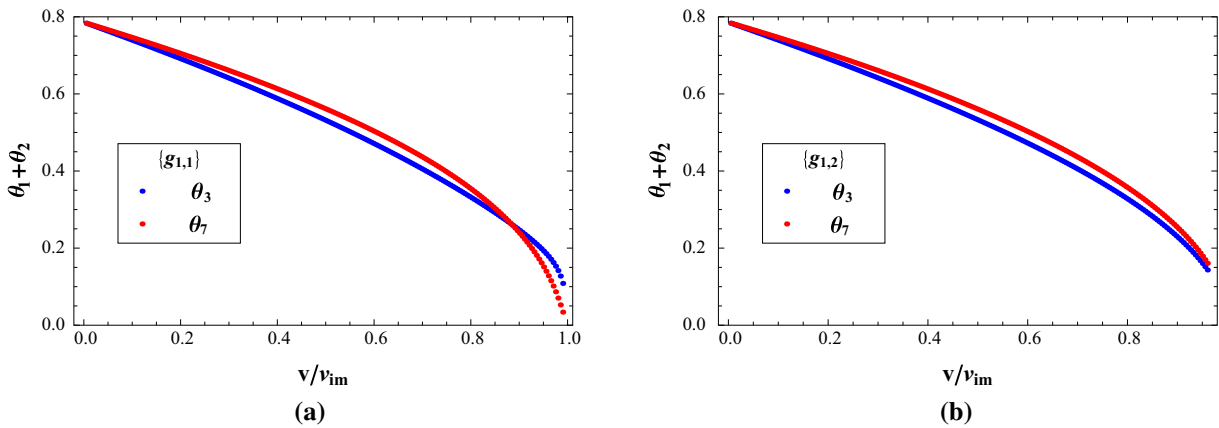

FIG. 12. BE test. Relative rotation of the fibres in central regions versus displacement. $H/W > 4$. First gradient energy models. **a** BE test. Relative rotation of the fibres in central regions versus displacement. $H/W > 4$. First gradient energy $g_{1,1}$. **b** BE test. relative rotation of the fibres in central regions versus displacement. $H/W > 4$. First gradient energy $g_{1,2}$

3.3. Concluding remarks for the analysis of the BE test

The load-displacement curve evaluated with the simplified kinematics adopted, once properly scaled, is independent on the slenderness ratio of the specimen. In the case the dominant strain energy depends on the gradient of the shear deformation an unstable behaviour is obtained. For all the other cases the response of the specimen is qualitatively very similar whatever strain energy is used.

Some difference is observed in the deformation of the specimen obtained with the first energy model, which is almost uniform along the whole sample, and with the second energy models, that presents a neck. The effect appears to be the more evident the greater is the slenderness of the specimen.

In consideration of the rather insensitivity to the different strain energy models of the response of the specimen subjected to the BE test, it appears that this test alone is not able to give sufficient indications
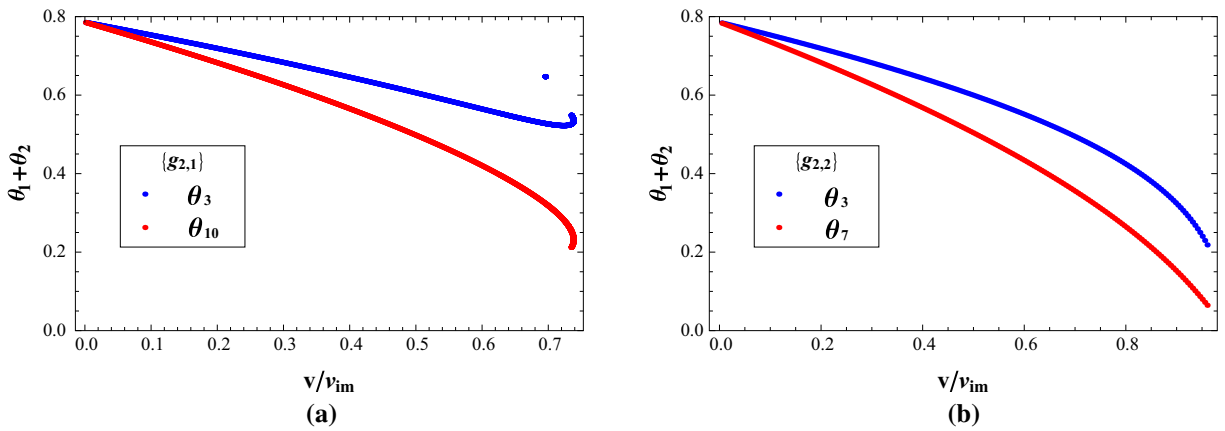
FIG. 13. BE test. Relative rotation of the fibres in central regions versus displacement. $H/W > 4$. Second gradient energy models. **a** BE test. Relative rotation of the fibres in central regions versus displacement. $H/W > 4$. Second gradient energy $g_{2,1}$. **b** BE test. Relative rotation of the fibres in central regions versus displacement. $H/W > 4$. Second gradient energy $g_{2,2}$
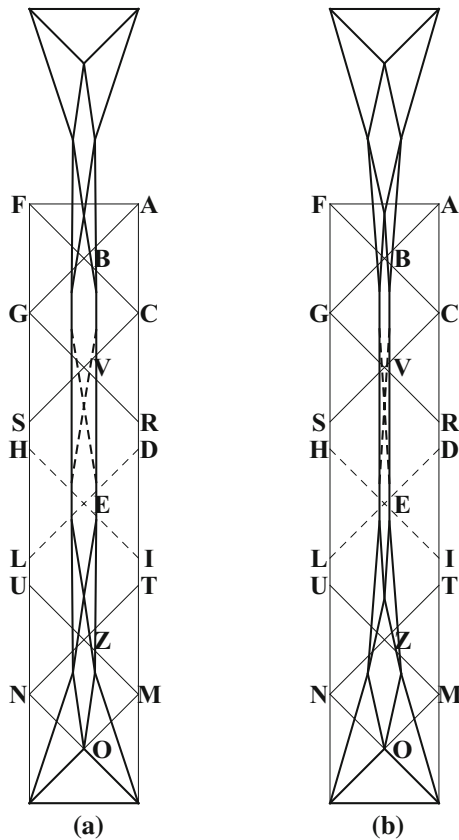

FIG. 14. BE test. Deformation of the sample. $H/W > 4$. **a** First gradient energy $g_{1,2}$. **b** Second gradient energy $g_{2,2}$

on the constitutive model most appropriate for the material under investigation. More tests are needed, involving different deformation modes.

In the following sections a generalized Bias Test will be proposed and analyzed using the same simplified geometric assumptions adopted in this section. It will be shown that qualitative differences may arise in some aspects of the deformation, which can help in the interpretation of the experimental results.

4. Modified bias test

In this section is examined the test represented in Fig. 15. The specimen, having the same shape and fibre orientation as the standard specimen for the BE test, is clamped at one end, while the opposite end is rotated of an angle ϕ around the corner A. Region "0" undergoes a rigid rotation, so that the coordinates of point B are determined by the rotation. As can be seen from the picture, each region of the specimen undergoes a different shear strain (apart from regions 0, 9 that do not deform, see Fig. 3 for the numbering of the regions).

We limit the analysis to the case of $2 \leq H/W < 4$. In the hypothesis that the fibres remain straight within each region, the deformation of the specimen can be determined as a function of the coordinates of the central point "E", that can be obtained minimizing the potential energy. The relative rotation of the fibres in region 3a and 3b can be obtained in a similar way to expression (10), considering separately the projection of the fibres on the axes BE and OE (the positions of the points B, O are known). Then the deformation so obtained for the sides of the regions 3a and 3b are rotated into the global reference system (rotation which depends only on the position of point E).
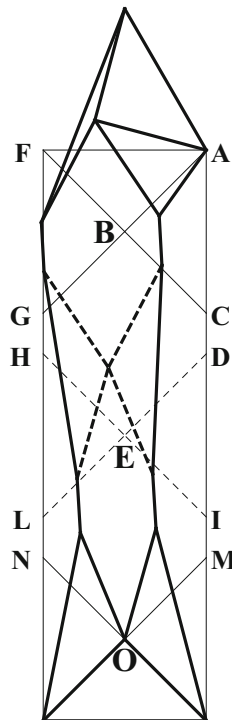

FIG. 15. Modified bias test. Schematic of the geometry of the test. $H/W < 4$
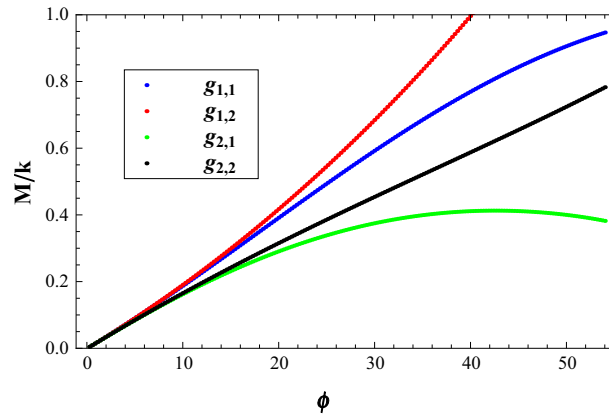
FIG. 16. Modified bias test. Moment rotation curves obtained with four choices for the strain energy. $H/W < 4$
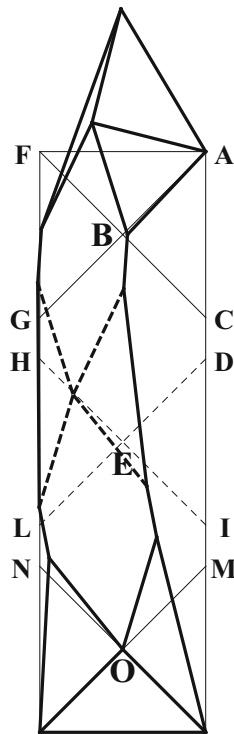

FIG. 17. Modified bias test. Deformed shape of the specimen, quadratic second gradient energy $g_{2,2}$. $H/W < 4$

A limit rotation is attained when the relative rotation in the region 1 is equal to $\pi/2$, that is, when the fibres get totally aligned and no further stretching is allowed. The limit value of the rotation angle depends on the position of point E (and thus on the solution of the minimization problem) and on the aspect ratio of the specimen. It ranges between 60° and 80°, the greater the more slender is the specimen.

Using a procedure analogous to the one illustrated for the BE test, the response of the specimen to a monotonically increasing rotation was calculated for the four energy forms defined in Sect. 2.1. The
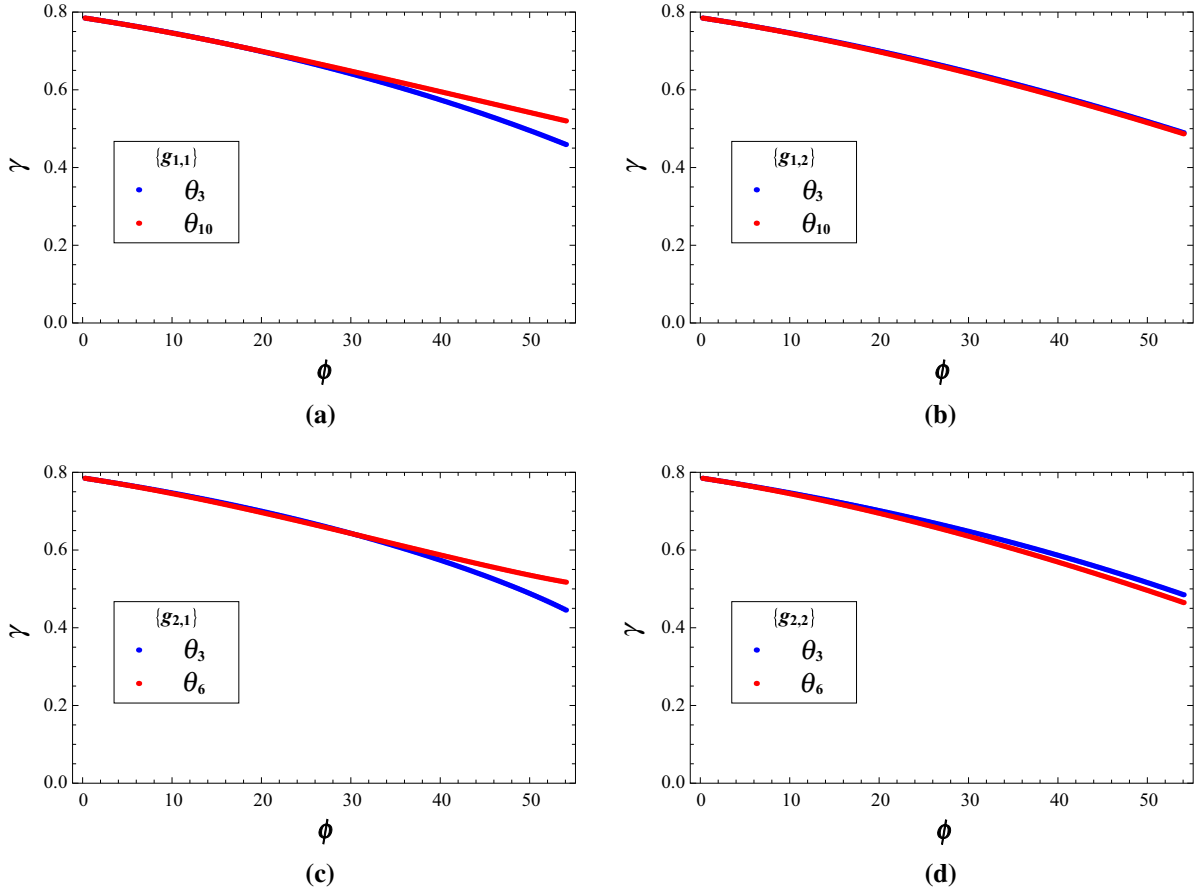
FIG. 18. Modified bias test. Relative rotation of the fibres in central regions versus rotation. All energy models. **a** Modified bias test. Relative rotation of the fibres in central regions versus rotation. First gradient energy $g_{1,1}$. **b** Modified bias. Relative rotation of the fibres in central regions versus rotation. First gradient energy $g_{1,2}$. **c** Modified bias test. Relative rotation of the fibres in central regions versus rotation. Second gradient energy $g_{2,1}$. **d** Modified bias test. Relative rotation of the fibres in central regions versus rotation. Second gradient energy $g_{2,2}$

reaction moment M at the rotating edge was obtained similarly to (17) as

$$M = \frac{\partial E_d}{\partial \phi} \tag{19}$$

The results are summarized in Fig. 16, limited to a maximum rotation of 60°. All the results have been normalized with respect to the initial slope. The top two curves refer to the results obtained with the first gradient energy (in the highest curve the energy used is $g_{1,2}$, in the other is $g_{1,1}$.) The bottom two curves refer to the second gradient energy, the lowest curve shows the results for the energy $g_{2,1}$, which presents a limit point followed by an unstable behaviour.

With respect to the case of the standard BE test the moment-rotation curves obtained present a greater difference among them, that can help to evaluate from experimental results what the most adequate constitutive relation might be.

The deformed shape of the specimen for a rotation close to the limit one obtained using the energy $g_{2,2}$ is presented in Fig. 17. It can be observed that according to the simplified hypotheses used in this work the shear in the central part of the specimen is nearly uniform. This is confirmed by the plots of
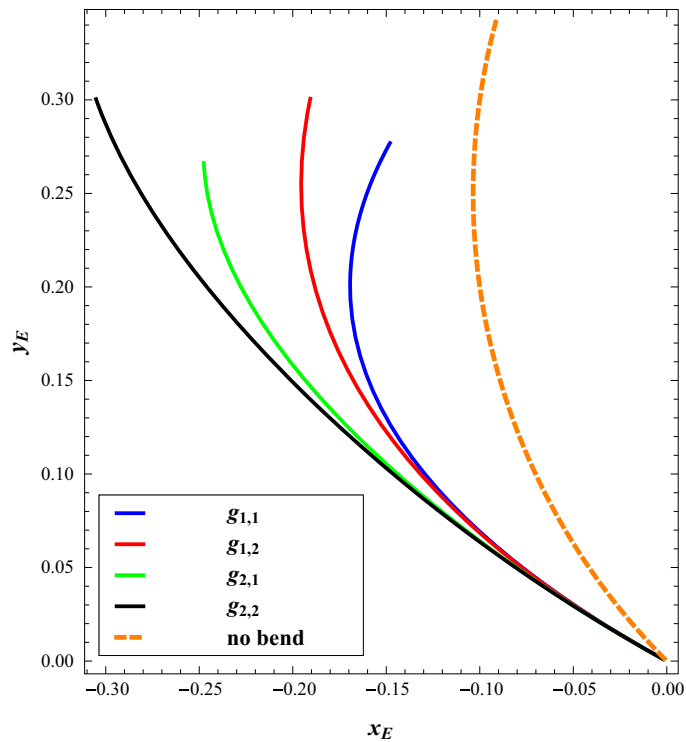
FIG. 19. Modified bias test. Trajectory of the coordinates of the central point "E" of the specimen. All energy models. The *dashed line* refers to the case of a deformation without bending.

Fig. 18 that show the relative rotation of the fibres in the central regions 3a and 3b, for the four cases examined. In all of them, the two rotations are almost equal, except for the case of the strain energy depending on the square of the shear, for very great values of the rotation angle.

Although the shears in the central region have been found to be almost uniform, the specimen does not undergo simple stretching, rather it presents bending, This effect can be appreciated from the trajectories of point E plotted in Fig. 19 for the four cases examined (solid lines) compared with the trajectory that the point would have if no bending were present, that is if the point E were always aligned to points B, O (dashed line). It can be seen that the greater deviations from the no bending condition occurs for the simulations obtained using the second gradient energy, and for large values of the rotation. Apparently, the case that presents more bending is when the strain energy is taken to depend directly from the curvature of the fibres. Also this appears to be a useful consideration for interpreting experimental results.

5. Conclusions

A simplified mechanical analysis of two tests performed on a strip of woven fibres with orthogonal yarns aligned at $45\,^\circ$ with the specimen axis. The fibres have been considered inextensible, so that the material experiences only shear deformation. A simplified kinematics has been adopted, such that the shear deformation is piecewise constant in the specimen. Two kinds of test have been examined, the standard Bias Extension Test and a modified version of it. It has been obtained the deformation and the force versus displacement curve adopting four different constitutive models for the material. In the simulations the strain energy has been assumed quadratic in the shear deformation or in the relative rotation, so

that the nonlinearity of the behaviour is of geometric nature only. In addition to first gradient energy models, it has been assumed that the deformation energy of the material can depend also on the strain gradient. This assumption allows to account for the bending of the fibres during the deformation, and thus to account in a simplified way for the microstructure of the composite.

The Bias Extension test has been examined first. It has been found that when the bending energy (the second gradient energy) is predominant, instabilities occur, and this could be related to the loss of stability observed in the experiments.

A modified Bias test has been analysed, in which the end of the specimen is rotated around one corner. It has been observed that the deformation depends on the slenderness of the specimen, and that the predictions of the energy models tested differ among themselves. In this case, bending has shown to arise in the specimen, in addition to stretching associated with the rotation of the fibres.

Plots of the relative rotations of the fibres at the centre of the specimen and at the vertex of the unde-formed region have also been presented, since those angles are usually measured during the experiments.

The results of the simplified analyses presented will help to interpret the results of more detailed simulations obtained with Finite Element Analysis that will be presented in a future work.

References

1. Spencer, A.J.M., Soldatos, K.P.: Finite deformations of fibre-reinforced elastic solids with fibre bending stiffness. Int. J. Non-Linear Mech. **42**(2), 355–368 (2007)
2. Nikopour, H., Selvadurai, A.: Torsion of a layered composite strip. Compos. Struct. **95**, 1–4 (2013)
3. Nikopour, H., Selvadurai, A.P.S.: Concentrated loading of a fibre-reinforced composite plate: experimental and compu-tational modeling of boundary fixity. Compos. B Eng. **60**, 297–305 (2014)
4. Grillo, A., Wittum, G., Tomic, A., Federico, S.: Remodelling in statistically oriented fibre-reinforced materials and biological tissues. Math. Mech. Solids **20**(9), 1107–1129 (2015). doi:10.1177/1081286513515265
5. Federico, S., Grillo, A.: Elasticity and permeability of porous fibre-reinforced materials under large deformations. Mech. Mater. **44**, 58–71 (2012)
6. Andreaus, U., Giorgio, I., Lekszycki, T.: A 2-D continuum model of a mixture of bone tissue and bio-resorbable material for simulating mass density redistribution under load slowly variable in time. ZAMM Z. Angew. Math. Mech. **94**(12), 978–1000 (2014)
7. Giorgio I., Andreaus U., Lekszycki T., Della Corte, A.: The influence of different geometries of matrix/scaffold on the remodeling process of a bone and bioresorbable material mixture with voids. Math. Mech. Solids (2015). doi:10.1177/1081286515616052
8. Nadler, B., Steigmann, D.J.: A model for frictional slip in woven fabrics. C. R. Mec. **331**(12), 797–804 (2003)
9. Giorgio, I., Scerrato, D.: Multi-scale concrete model with rate-dependent internal friction. Eur. J. Environ. Civ. Eng. (2016). doi:10.1080/19648189.2016.1144539
10. Placidi, L., Andreaus, U., Della Corte, A., Lekszycki, T.: Gedanken experiments for the determination of two-dimensional linear second gradient elasticity coefficients. Z. Angew. Math. Phys. **66**(6), 3699–3725 (2015)
11. Lekszycki, T., Olhoff, N., Pedersen, J.J.: Modelling and identification of viscoelastic properties of vibrating sandwich beams. Compos. Struct. **22**(1), 15–31 (1992)
12. Andreaus, U., Chiaia, B., Placidi, L.: Soft-impact dynamics of deformable bodies. Contin. Mech. Thermodyn. **25**(2–4), 375–398 (2013)
13. Placidi, L.: A variational approach for a nonlinear one-dimensional damage-elasto-plastic second-gradient continuum model. Contin. Mech. Thermodyn. **28**(1–2), 119–137 (2016)
14. Placidi, L.: A variational approach for a nonlinear 1-dimensional second gradient continuum damage model. Contin. Mech. Thermodyn. **27**(4–5), 623–638 (2015)
15. Misra, A., Singh, V.: Micromechanical model for viscoelastic materials undergoing damage. Contin. Mech. Thermo-dyn. **25**(2–4), 343–358 (2013)
16. Roveri, N., Carcaterra, A.: Damage detection in structures under traveling loads by Hilbert–Huang transform. Mech. Syst. Signal Process. **28**, 128–144 (2012)
17. Harrison, P., Wiggers, J., Long, A.: Normalization of shear test data for rate-independent compressible fabrics. J. Compos. Mater. **42**, 2315–2344 (2008)
18. Bassett, R., Postle, R., Pan, N.: Experimental methods for measuring fabric mechanical properties. Rev. Anal. Text. Res. J. **69**(11), 866–875 (1999)

19. Taha, I., Abdin, Y., Ebeid, S.: Comparison of picture frame and Bias-Extension tests for the characterization of shear behaviour in natural fibre woven fabrics. Fibers Polym. **14**(2), 338–344 (2013)

20. Sharma, S., Sutcliffe, M., Chang, S.: Characterisation of material properties for draping of dry woven composite material. Compos. A **34**, 1167–1175 (2003)

21. Luongo, A., Zulli, D., Piccardo, G.: A linear curved-beam model for the analysis of galloping in suspended cables. J. Mech. Mater. Struct. **2**(4), 675–694 (2007)

22. Piccardo, G., Pagnini, L.C., Tubino, F.: Some research perspectives in galloping phenomena: critical conditions and post-critical behavior. Contin. Mech. Thermodyn. **27**(1–2), 261–285 (2015)

23. Pignataro, M., Rizzi, N., Ruta, G., Varano, V.: The effects of warping constraints on the buckling of thin-walled structures. J. Mech. Mater. Struct. **4**(10), 1711–1727 (2010)

24. Bersani, A.M., Giorgio, I., Tomassetti, G.: Buckling of an elastic hemispherical shell with an obstacle. Contin. Mech. Thermodyn. **25**(2–4), 443–467 (2013)

25. Rizzi, N.L., Varano, V., Gabriele, S.: Initial postbuckling behavior of thin-walled frames under mode interaction. Thin Walled Struct. **68**, 124–134 (2013)

26. AminPour, H., Rizzi, N.: A one-dimensional continuum with microstructure for single-wall carbon nanotubes bifurcation analysis. Math. Mech. Solids **21**(2), 168–181 (2016)

27. Gabriele, S., Rizzi, N., Varano, V.: On the imperfection sensitivity of thin-walled frames. In: Proceedings of the Eleventh International Conference on Computational Structures Technology. Civil-Comp Press, Stirlingshire (2012)

28. Rizzi, N., Varano, V.: On the postbuckling analysis of thin-walled frames. In: Thirteenth International Conference on Civil, Structural and Environmental Engineering Computing. Civil-Comp Press (2011)

29. Pignataro, M., Ruta, G., Rizzi, N., Varano, V.: Effects of warping constraints and lateral restraint on the buckling of thin-walled frames. In: ASME 2009 International Mechanical Engineering Congress and Exposition, pp. 803–810. American Society of Mechanical Engineers (2009)

30. Lomov, S., Barburski, M., Stoilova, T., Verpoest, I., Akkerman, R., Loendersloot, R., Ten Thije, R.: Carbon composites based on multiaxial multiply stitched preforms. Part 3. Biaxial tension, picture frame and compression tests of the preforms. Compos. A **26**, 1188–1206 (2005)

31. Milani, A., Nemes, J., Lebrun, G., Bureau, M.: A comparative analysis of a modified picture frame test for characterization of woven fabrics. Polym. Compos. **31**(4), 561–568 (2009)

32. Domskiené, J., Strazdiené, E.: Investigation of fabric shear behaviour. Fibres Text. East. Eur. **13**(26–30), 561–568 (2005)

33. Harrison, P., Clifford, M., Long, A.: Shear characterisation of viscous woven textile composites: a comparison between picture frame and bias extension experiments. Compos. Sci. Technol. **64**, 1453–1465 (2004)

34. Härtel, F., Harrison, P.: Evaluation of normalisation methods for uniaxial bias extension tests on engineering fabrics. Compos. A **37**, 61–69 (2014)

35. Lee, W., Padvoiskis, J., Cao, J., Luycker, E.de , Boisse, P., Morestin, F., Chen, J., Sherwood, J.: Bias-extension of woven composite fabrics. Int. J. Mater. Form. **1(suppl. 1)**, 895–898 (2008)

36. Cao, J., Akkerman, R., Boisse, P., Chen, J., Cheng, H., Graaf, E.de , Gorczyca, J., Harrison, P., Hivet, G., Launay, J., Lee, W., Liu, L., Lomov, S., Long, A., Luycker, E. de , Morestin, F., Padvoiskis, J., Peng, X., Sherwood, J., Stoilova, T., Tao, X., Verpoest, I., Willems, A., Wiggers, J., Yu, T., Zhu, B.: Characterization of mechanical behavior of woven fabrics: experimental methods and benchmark results. Compos. A **39**, 1037–1053 (2008)

37. Hivet, G., Duong, A.V.: A contribution to the analysis of the intrinsic shear behaviour of fabrics. J. Compos. Mater. **45**(6), 695–717 (2011)

38. Launay, J., Hivet, G., Duong, A., Boisse, P.: Experimental analysis of the influence of tensions on in plane shear behaviour of woven composite reinforcements. Compos. Sci. Technol. **68**(2), 506–515 (2008)

39. Lomov, S., Verpoest, I.: Model of shear of woven fabric and parametric description of shear resistance of glass woven reinforcements. Compos. Sci. Technol. **66**(7–8), 919–923 (2006)

40. Lee, W., Cao, J., Badel, P., Boisse, P.: Non-orthogonal constitutive model for woven composites incorporating tensile effect on shear behavior. Int. J. Mater. Form. **1(suppl. 1)**, 891–894 (2008)

41. Harrison, P., Abdiwi, F., Guo, Z., Potluri, P., Yu, W.: Characterising the shear-tension coupling and wrinkling behaviour of woven engineering fabrics. Compos. A **43**(6), 903–914 (2012)

42. Harrison, P.: Normalisation of biaxial bias extension test results considering shear tension coupling. Compos. A **43**, 1546–1554 (2012)

43. Boisse, P., Borr, M., Buet, K., Cherouat, A.: Finite element simulations of textile composite forming including the biaxial fabric behavior. Compos. B **28**(41), 453–4644 (1997)

44. dell'Isola, F., Cuomo, M., Greco, L., Della Corte, A.: Bias extension test for pantographic sheets: numerical simulations based on second gradient shear energies. (submitted)

45. Carcaterra, A., dell'Isola, F., Esposito, R., Pulvirenti, M.: Macroscopic description of microscopically strongly inhomogenous systems: a mathematical basis for the synthesis of higher gradients metamaterials. Arch. Ration. Mech. Anal. **218**(3), 1239–1262 (2015)

46. Alibert, J.-J., Della Corte, A.: Second-gradient continua as homogenized limit of pantographic microstructured plates: a rigorous proof. Z. Angew. Math. Phys. **66**(5), 2855–2870 (2015)

47. Pideri, C., Seppecher, P.: A second gradient material resulting from the homogenization of an heterogeneous linear elastic medium. Contin. Mech. Thermodyn. **9**(5), 241–257 (1997)

48. Cecchi, A., Rizzi, N.L.: Heterogeneous elastic solids: a mixed homogenization-rigidification technique. Int. J. Solids Struct. **38**(1), 29–36 (2001)

49. Goda, I., Assidi, M., Ganghoffer, J.-F.: Equivalent mechanical properties of textile monolayers from discrete asymptotic homogenization. J. Mech. Phys. Solids **61**(12), 2537–2565 (2013)

50. Rahali, Y., Giorgio, I., Ganghoffer, J., dell'Isola, F.: Homogenization à la Piola produces second gradient continuum models for linear pantographic lattices. Int. J. Eng. Sci. **97**, 148–172 (2015)

51. Soubestre, J., Boutin, C.: Non-local dynamic behavior of linear fiber reinforced materials. Mech. Mater. **55**, 16–32 (2012)

52. Zhang, Z., Wang, C.M., Challamel, N., Elishakoff, I.: Obtaining Eringen s length scale coefficient for vibrating nonlocal beams via continualization method. J. Sound Vib. **333**(20), 4977–4990 (2014)

53. Challamel, N., Wang, C.M., Elishakoff, I.: Discrete systems behave as nonlocal structural elements: bending, buckling and vibration analysis. Eur. J. Mech. A Solids **44**, 125–135 (2014)

54. Pipkin, A.: Some developments in the theory of inextensible networks. Q. Appl. Math. **38**(3), 343–355 (1980)

55. Pipkin, A.: Plane traction problems for inextensible networks. Q. J. Mech. Appl. Math. **34**(4), 415–429 (1981)

56. Rivlin, R.: Plane strain of a net formed by inextensible chords. J. Ration. Mech. Anal. **4**(6), 951–974 (1955)

57. dell'Isola, F., Steigmann, D.: A two-dimensional gradient-elasticity theory for woven fabrics. J. Elast. **118**(1), 113–125 (2015)

58. Steigmann, D.J., dell'Isola, F.: Mechanical response of fabric sheets to three-dimensional bending, twisting, and stretching. Acta Mech. Sin. **31**(3), 373–382 (2015)

59. dell'Isola, F., Steigmann, D., Della Corte, A.: Synthesis of fibrous complex structures: designing microstructure to deliver targeted macroscale response. Appl. Mech. Rev. **67**(6), 060804 (2016)

60. dell'Isola, F., Della Corte, A., Giorgio, I., Scerrato, D.: Pantographic 2D sheets: discussion of some numerical investigations and potential applications. Int. J. Non-Linear Mech. (2015). doi:10.1016/j.ijnonlinmec.2015.10.010

61. dell'Isola, F., Della Corte, A., Greco, L., Luongo, A.: Plane bias extension test for a continuum with two inextensible families of fibers: A variational treatment with Lagrange multipliers and a perturbation solution. Int. J. Solids Struct. **81**, 1–12 (2016)

62. dell'Isola, F., Lekszycki, T., Pawlikowski, M., Grygoruk, R., Greco, L.: Designing a light fabric metamaterial being highly macroscopically tough under directional extension: first experimental evidence. Z. Angew. Math. Phys. **66**(6), 3473–3498 (2015)

63. dell'Isola, F., Giorgio, I., Pawlikowski, M., Rizzi, N.L.: Large deformations of planar extensible beams and pantographic lattices: heuristic homogenization, experimental and numerical examples of equilibrium. Proc. R. Soc. A **472**(2185), 20150790 (2016)

64. dell'Isola, F., Seppecher, P., Della Corte, A.: The postulations á la D'Alembert and á la Cauchy for higher gradient continuum theories are equivalent: a review of existing results. Proc. R. Soc. A **471**(2183), 20150415 (2015)

65. dell'Isola, F., Andreaus, U., Placidi, L.: At the origins and in the vanguard of peridynamics, non-local and higher-gradient continuum mechanics: an underestimated and still topical contribution of Gabrio Piola. Math. Mech. Solids **20**(8), 887–928 (2015)

66. Rosi, G., Giorgio, I., Eremeyev, V.A.: Propagation of linear compression waves through plane interfacial layers and mass adsorption in second gradient fluids. ZAMM Z. Angew. Math. Mech. **93**(12), 914–927 (2013)

67. Bleustein, J.L.: A note on the boundary conditions of Toupin's strain-gradient theory. Int. J. Solids Struct. **3**(6), 1053–1057 (1967)

68. Del Vescovo, D., Giorgio, I.: Dynamic problems for metamaterials: review of existing models and ideas for further research. Int. J. Eng. Sci. **80**, 153–172 (2014)

69. Koiter, W.T.: Couple stresses in the theory of elasticity, I and II. Proc. Kon. Ned. Akad. Wet. Ser. B. **67**(1), 17–44 (1964)

70. Altenbach, H., Eremeyev, V.A.: On the linear theory of micropolar plates. ZAMM J. Appl. Math. Mech. **89**(4), 242–256 (2009)

71. Altenbach, J., Altenbach, H., Eremeyev, V.A.: On generalized Cosserat-type theories of plates and shells: a short review and bibliography. Arch. Appl. Mech. **80**(1), 73–92 (2010)

72. Eremeyev, V.A., Pietraszkiewicz, W.: Material symmetry group of the non-linear polar-elastic continuum. Int. J. Solids Struct. **49**(14), 1993–2005 (2012)

73. Placidi, L., Giorgio, I., Della Corte, A., Scerrato, D.: Euromech 563 Cisterna 678 di Latina 17–21 March 2014 Generalized continua and their applications to the de679 sign of composites and metamaterials: a review of presentations and discussions. Math. Mech. Solids (2015). doi:10.1177/1081286515576948

74. Berezovski, A., Giorgio, I., Della Corte, A.: Interfaces in micromorphic materials: wave transmission and reflection with numerical simulations. Math. Mech. Solids **21**(1), 37–51 (2016)

75. Greco, L., Cuomo, M.: An isogeometric implicit G1 mixed finite element for Kirchhoff space rods. Comput. Methods Appl. Mech. Eng. **298**, 325–349 (2016)
76. Cazzani, A., Malagù, M., Turco, E.: Isogeometric analysis of plane-curved beams. Math. Mech. Solids (2014). doi:10.1177/1081286514531265
77. Cazzani, A., Malagù, M., Turco, E., Stochino, F.: Constitutive models for strongly curved beams in the frame of isogeometric analysis. Math. Mech. Solids **21**, 183–209 (2016)
78. Fischer, P., Klassen, M., Mergheim, J., Steinmann, P., Müller, R.: Isogeometric analysis of 2D gradient elasticity. Comput. Mech. **47**(3), 325–334 (2011)
79. Della Corte, A., Battista, A., dell'Isola, F.: Referential description of the evolution of a 2D swarm of robots interacting with the closer neighbors: perspectives of continuum modeling via higher gradient continua. Int. J. Non-Linear Mech. **80**, 209–220 (2016)

M. Cuomo
Dipartimento di ingegneria Civile e Architettura (DICAR)
Università degli Studi di Catania
Catania
Italy

F. dell'Isola
Dipartimento di Ingegneria Strutturale e Geotecnica (DISG)
Università di Roma La Sapienza
Rome
Italy

M. Cuomo · F. dell'Isola · L. Greco
International Research Center for the Mathematics
and Mechanics of Complex Systems (MeMoCS)
Università dell'Aquila
Cisterna di Latina
Italy
e-mail: leopoldo.greco@virgilio.it